Chinese Physics B

中国物理学会
Chinese Physical Society

RAPID COMMUNICATION

Intercalation of van der Waals layered materials: A route towards engineering of electron correlation*

To cite this article: Jingjing Niu *et al* 2020 *Chinese Phys. B* **29** 097104

Chin. Phys. B Vol. 29, No. 9 (2020) 097104

RAPID COMMUNICATION

Intercalation of van der Waals layered materials: A route towards engineering of electron correlation[*]

Jingjing Niu(牛晶晶)[1,2,†], Wenjie Zhang(章文杰)[1,2,†], Zhilin Li(李治林)[1,2,†], Sixian Yang(杨嗣贤)[3], Dayu Yan(闫大禹)[4], Shulin Chen(陈树林)[5], Zhepeng Zhang(张哲朋)[6], Yanfeng Zhang(张艳锋)[6], Xinguo Ren(任新国)[3], Peng Gao(高鹏)[2,5,7], Youguo Shi(石友国)[4], Dapeng Yu(俞大鹏)[1,2,8], and Xiaosong Wu(吴孝松)[1,2,8,‡]

[1] State Key Laboratory for Artificial Microstructure and Mesoscopic Physics, Beijing Key Laboratory of Quantum Devices, Peking University, Beijing 100871, China
[2] Collaborative Innovation Center of Quantum Matter, Beijing 100871, China
[3] CAS Key Laboratory of Quantum Information, Synergetic Innovation Center of Quantum Information and Quantum Physics, University of Science and Technology of China, Hefei 230026, China
[4] Institute of Physics and Beijing National Laboratory for Condensed Matter Physics, Chinese Academy of Sciences, Beijing 100190, China
[5] Electron Microscopy Laboratory, School of Physics, Peking University, Beijing 100871, China
[6] Center for Nanochemistry, Beijing National Laboratory for Molecular Sciences, College of Chemistry and Molecular Engineering, Peking University, Beijing 100871, China
[7] International Center for Quantum Materials, School of Physics, Peking University, Beijing 100871, China
[8] Department of Physics, Southern University of Science and Technology of China, Shenzhen 518055, China

(Received 11 July 2020; revised manuscript received 28 July 2020; accepted manuscript online 1 August 2020)

Being parent materials of two-dimensional (2D) crystals, van der Waals layered materials have received revived interest. In most 2D materials, the interaction between electrons is negligible. Introducing the interaction can give rise to a variety of exotic properties. Here, via intercalating a van der Waals layered compound VS_2, we find evidence for electron correlation by extensive magnetic, thermal, electrical, and thermoelectric characterizations. The low temperature Sommerfeld coefficient is 64 mJ$\cdot$K$^{-2}\cdot$mol^{-1} and the Kadowaki–Woods ratio $r_{\mathrm{KW}} \sim 0.20a_0$. Both supports an enhancement of the electron correlation. The temperature dependences of the resistivity and thermopower indicate an important role played by the Kondo effect. The Kondo temperature T_{K} is estimated to be around 8 K. Our results suggest intercalation as a potential means to engineer the electron correlation in van der Waals materials, as well as 2D materials.

Keywords: V_5S_8, intercalation, Kondo lattice, strong correlations

PACS: 71.27.+a, 75.30.Mb, 71.20.Tx **DOI:** 10.1088/1674-1056/abab85

1. Introduction

Strong electron correlations can give rise to many exotic properties in materials, such as high temperature superconductivity, heavy fermions, quantum spin liquids, etc.[1–3] Understanding the effect has been a grand challenge in condensed matter physics. An example of a strongly correlated electron system under extensive study is the Kondo lattice, in which a dense array of local magnetic moments interact with itinerant conduction electrons via the so-called Kondo effect. The competition between the Kondo effect, which results in screening of the local moment, and the Ruderman–Kittel–Kasuya–Yoshida (RKKY) interaction, which promotes ordering of the moment, leads to a variety of ground states, e.g., a Kondo insulator, an antiferromagnet, and a heavy fermion superconductor.[2,4–13]

Note that the key ingredients of a Kondo lattice include local moments and itinerant electrons. A naive idea to design such a material is to embed an array of moments in a conductive material. Here, we demonstrate that this simple route is feasible by introducing the Kondo effect into a nonmagnetic van der Waals layered material via intercalation with local moments. We study V_5S_8 (or $V_{1/4}VS_2$), a self-intercalated compound of VS_2. The magnetic susceptibility, specific heat, electrical and thermoelectric transport studies coherently suggest Kondo physics at work and the consequent enhancement of electron correlation in V_5S_8. Intercalation of van der Waals materials has been well studied, for instance, in graphite and transition metal chalcogenides.[14–16] Various chemical species with very different properties can be intercalated. Given a large body of van der Waals materials, we believe that this technique can be a versatile means to introduce a class of Kondo lattices. Moreover, the same idea can be applied to two-dimensional materials, too.[17,18]

---

[*] Project supported by the National Key Basic Research Program of China (Grant Nos. 2013CBA01603, 2016YFA0300600, and 2016YFA0300903), the National Natural Science Foundation of China (Grant Nos. 11574005, 11774009, 11222436, and 11574283), and the National Postdoctoral Program for Innovative Talents of China (Grant No. BX201700012) funded by China Postdoctoral Science Foundation.

[†] These authors contributed equally.

[‡] Corresponding author. E-mail: xswu@pku.edu.cn

2. Experimental techniques

2.1. Methods

V_5S_8 bulk single crystals were grown by a chemical vapor transport method, using vanadium and sulfur powders as precursors and iodine as a transport agent. These species were loaded into a silica ampule under argon. The ampule was then evacuated, sealed, and heated gradually in a two-zone tube furnace to a temperature gradient of 1000 °C to 850 °C. After two weeks, single crystals with regular shapes and shiny facets can be obtained. X-ray experiments on grown crystals indicate a pure V_5S_8 phase. The crystallographic structure of the single crystal was further confirmed by high-angle annular dark field scanning transmission electron microscope (HAADF-STEM). Transport properties were measured using a standard lock-in method in an Oxford variable temperature cryostat from 1.5 K to 300 K. Heat capacity was measured in a Quantum Design physical properties measurement system. A Quantum Design SQUID magnetometer was employed to measure the magnetic susceptibility. Thermopower of bulk single crystals was measured using a standard four-probe steady-state method with a Chromel/AuFe(0.07%) thermocouple.

2.2. Structure

V_5S_8 can be seen as a van der Waals layered material VS_2 self-intercalated with V, i.e., $V_{1/4}VS_2$. It crystallizes in a monoclinic structure, space group $C2/m$. V atoms lie on three inequivalent sites. Intercalated V atoms take the V^{I} site, while V atoms in the VS_2 layer take V^{II} and V^{III} sites. Each V^{I} atom is surrounded by six S atoms, forming a distorted octahedron, shown in Fig. 1(b). The resultant crystal field is believed to be intricately related to the local magnetic moment of V atoms.[19,20] Figure 1(a) shows a HAADF-STEM image of a single crystal, in which both V and S atoms can be clearly seen, as well as the rectangular arrangement of the intercalated V^{I} atoms. Images have been taken at various spots. All of them show high crystallinity and the same lattice orientation, indicating uniform V intercatlation (see Fig. A1 in Appendix A). A zoom-in and color-enhanced image is shown in the lower right of Fig. 1(a), which is in excellent accordance with the in-plane atomic model of V_5S_8. The lattice constants, $a = 11.65$ Å and $b = 6.76$ Å, are determined from a fast Fourier transformation (FFT) image shown in the upper right of Fig. 1(a).

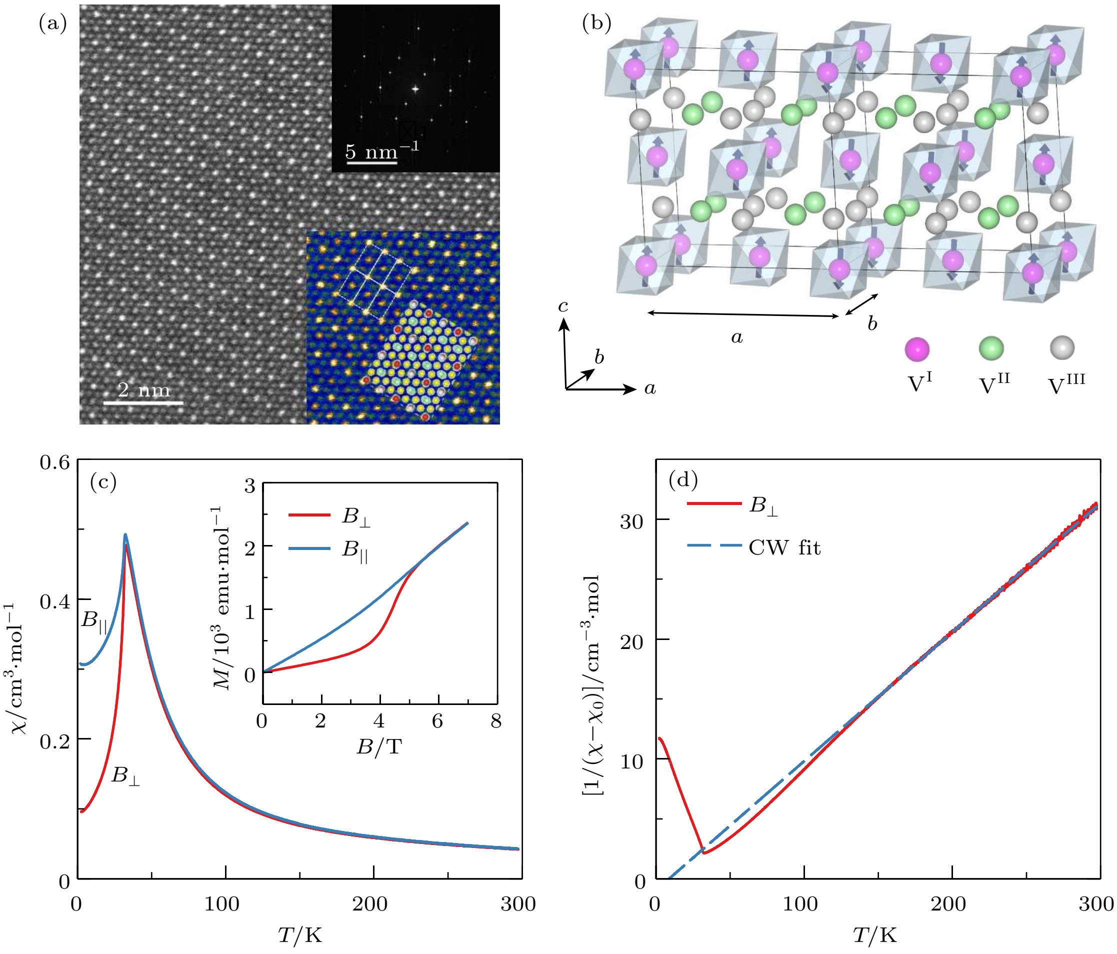

Fig. 1. Structural and magnetic properties of V_5S_8 bulk single crystal. (a) HAADF-STEM image. Lower inset, a zoom-in image with the in-plane atomic model. Upper inset, a reduced FFT image. (b) The magnetic unit cell with the $V^{I}S_6$ octahedron. The blue arrows indicate the direction of the magnetic moments on V^{I} sites. (c) The molar magnetic susceptibility χ for $B_{\perp}$ ($B \perp ab$ plane) and $B_{\parallel}$ ($B \parallel ab$ plane). The inset shows the low temperature ($T = 2$ K) isothermal magnetization curves. (d) The inverse magnetic susceptibility $1/(\chi - \chi_0)$ for $B_{\perp}$. The blue dashed line is a linear fit of the Curie–Weiss law, which gives $\theta = 8.8$ K, $\chi_0 = 0.01$ cm^3·mol^{-1}, and $\mu_{\mathrm{eff}} = 2.43\mu_{\mathrm{B}}$ per V^{I}.

2.3. Magnetic properties

VS_2 is a non-magnetic layered TMD.[21] V_5S_8, however, becomes an antiferromagnetic (AFM) metal because of the local moment of the intercalated V ion. The magnetic susceptibility of V_5S_8 displays a paramagnetic behavior which follows the Curie–Weiss (CW) law at high temperatures and undergoes an antiferromagnetic transition at about 32 K, shown in Fig. 1.[22] The high temperature CW behavior indicates local moments. Fitting of the paramagnetic susceptibility to the CW law, $\chi = \chi_0 + \frac{C}{T-\theta_{\rm CW}}$, yields a positive CW temperature $\theta_{\rm CW} \approx 8.8$ K despite the AFM order and an effective magnetic moment of $\mu_{\rm eff} = 2.43\mu_{\rm B}$ per V_5S_8 formula unit (f.u.). This value is consistent with the reported ones, ranging from $2.12\mu_{\rm B}$ to $2.49\mu_{\rm B}$.[22–24] It is generally believed that only $V^{\rm I}$ ions carry a local magnetic moment.[19,20,25] So, the measured moment is close to the theoretical value $2.64\mu_{\rm B}$ for $V^{3+}(3d^2)$.[19,22,26] Below the Néel temperature, the moments point in the direction of 10.4° away from the c axis toward the a axis. They align as $\uparrow\uparrow\downarrow\downarrow$ along the a axis, while ferromagnetically aligned along the b and c axes.[19] Consequently, the in-plane ($B \parallel ab$ plane) susceptibility is larger than the out-of-plane one. The field dependence of the out-of-plane magnetization displays a sudden change of the slope at about 4.5 T, seen in the inset of Fig. 1(c). This is caused by a metamagnetic spin-flop transition.[22] Taking the measured paramagnetic moment of $2.43\mu_{\rm B}$, $S \approx 0.8$ is obtained, close to the expected value $2S = 1.7$.[27] However, below $T_{\rm N}$, this moment was found to be smaller than expected, $0.7\mu_{\rm B}$ by neutron scattering or $0.22\mu_{\rm B}$ by nuclear magnetic resonance.[25,28] This discrepancy has been an unresolved puzzle. We would also like to point out that the susceptibility deviates from the CW law below 140 K. In the following, we are going to show that this puzzle and the deviation can be explained in terms of hybridization of the local d-electrons on $V^{\rm I}$ with the conduction electrons in the VS_2 plane, a correlation effect known as the Kondo effect.

2.4. Specific heat

There have already been indications for interactions between the localized d-electrons and the conduction electrons in this system. Anomalous Hall effect, due to skew scattering of conduction electrons off from local moments, has been observed in V_5S_8.[29] Photoemission-spectroscopy study has shown both local-moment-like and band-like features for V 3d electrons. To understand the discrepancy, it was thus postulated that the 3d electron that provides the local moment becomes partially itinerant at low temperatures.[20] Recently, the Kondo effect has been observed in similar compounds, VSe_2 with dilute V intercalation[30] and VTe_2 nanoplate.[31] In V_5S_8, where local moments of $V^{\rm I}$ atoms arrange in a periodic array, a Kondo lattice may even emerge. It is expected that the effective mass of the conduction electron will be enhanced by the electron correlation. We have carried out specific heat measurements. The data of a 3.18 mg bulk single crystal are presented in Fig. 2(a). A sizeable jump at $T_{\rm N} = 32$ K manifests the AFM transition. In the inset of Fig. 2(a), $C(T)/T$ is plotted as a function of T^2. By a linear fit to $C/T = \gamma + \beta T^2$, the electronic Sommerfeld coefficient, $\gamma = 74$ mJ·K^{-2} per mole of $V^{\rm I}$ atoms, is obtained, as is commonly done.[2,6,32,33]

Since the system exhibits an antiferromagnetic order, to obtain γ more accurately, one needs to consider the contribution from spin waves. So, the total specific heat at low temperatures consists of three parts,

$$C = \gamma T + \beta T^3 + B\sqrt{T}{\rm e}^{-\Delta/T}, \tag{1}$$

where βT^3 represents the phonon contribution. Generally, T^3 is a good approximation of the Debye model at low temperatures. The third term is the spin wave contribution, in which B is a prefactor and Δ is the spin wave gap.[34,35] To avoid having too many parameters when fitting the low T data to Eq. (1), we first estimate β from the data above $T_{\rm N}$. According to the Debye model, the full formula of the phonon contribution $C_{\rm la}$ can be written as[36]

$$C_{\rm la} = 9NR\left(\frac{T}{\theta_{\rm D}}\right)^3 \int_0^{\theta_{\rm D}/T} \frac{x^4{\rm e}^x}{({\rm e}^x-1)^2}{\rm d}x, \tag{2}$$

where N is the number of atoms in a f.u., R is the mole gas constant, and $\theta_{\rm D}$ is the Debye temperature. At temperature much higher than $T_{\rm N}$, the specific heat is dominated by the sum of the electronic and lattice contributions, $C = C_{\rm e} + C_{\rm la}$.[37] $C_{\rm mag}$ is relatively small, because it is described by the Schottky formula[38] or the Schotte & Schotte formula,[39,40] and decays rapidly with temperature.[36] Fitting high-T data to this sum yields $\theta_{\rm D} \sim 475$ K. Although the linear-T dependence of $C_{\rm e}$ needs to be included to obtain a good fit, the fitted $\theta_{\rm D}$ is not acutely sensitive to the linear term. Data for different samples with different γ produce essentially the same Debye temperature. $\beta = 0.235$ mJ/mol·K^4 can be calculated from $\beta = 12NR\pi^4/5\theta_{\rm D}^3$.

Once β is determined, C at low temperatures is fitted to Eq. (1). In Fig. 2(b), we plot the three contributions to the total specific heat according to the fitting results. The fitted γ is 64 mJ·K^{-2}·mol^{-1}, close to the one by the fit to $C/T = \gamma + \beta T^2$. Though much smaller than those in some f-electron heavy-fermion systems,[6] the γ value is still comparable to that of some strongly correlated materials.[32,33] The suppression of the Sommerfeld coefficient by magnetic ordering is typical in heavy fermion systems that order magnetically at low temperatures.[6,32] This is because of the competition between the Kondo coupling and the RKKY interaction.[4]

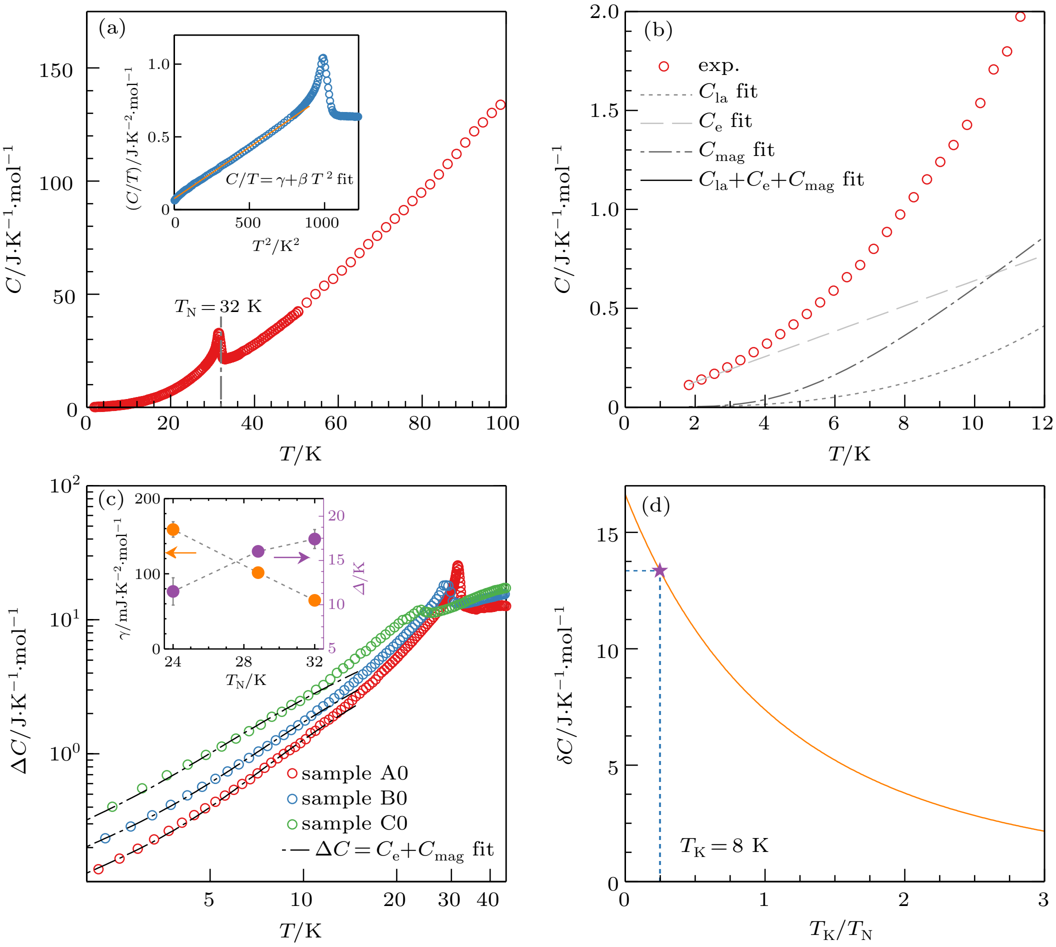

Fig. 2. Specific heat. (a) The specific heat C as a function of temperature. The inset shows a C/T versus T^2 plot. The solid line is a linear fit, which yields $\gamma = 74$ mJ·K^{-2}·mol^{-1}. (b) The low-T specific heat. $C_{\rm e}$ (dashed line) is the linear term γT deduced from (a); the lattice contribution (dotted line), $C_{\rm la} = \beta T^3$, is inferred from the Debye model fitting; the magnetic term $C_{\rm mag}$ (dash-dot line) is extracted by the fitting to Eq. (1). The sum of all three contributions, that is, the fitting curve using Eq. (1) (the solid line) is in good agreement with the experimental data (red circles). (c) The non-lattice part of specific heat ΔC for three types of samples with different $T_{\rm N}$. The dashed lines are the fits using Eq. (1) without βT^3. The inset shows the fitting parameters as a function of $T_{\rm N}$. (d) The relationship between the discontinuity of specific heat at $T_{\rm N}(\delta C)$ and $T_{\rm K}/T_{\rm N}$.

Such competition is reflected in the observed negative correlation between γ and $T_{\rm N}$. In Fig. 2(c), the specific heat analysis has been carried out for three samples. These samples display a variation of $T_{\rm N}$, likely due to different intercalation levels.[22] As $T_{\rm N}$ decreases, the spin-wave gap Δ is gradually reduced, but γ increases from 64 mJ·K^{-2}·mol^{-1} to 158 mJ·K^{-2}·mol^{-1}. Such a negative correlation is illustrated in the Doniach phase diagram of heavy fermion systems, indicating approaching to the quantum critical point.[4] Similar behavior has been observed in Kondo systems with a magnetic order.[41,42]

In order to better understand the Kondo scale in this system, we estimate the Kondo temperature $T_{\rm K}$ by the jump of the specific heat (δC) at the Néel temperature $T_{\rm N}$. According to the mean field theory, without Kondo coupling, the discontinuity in the specific heat δC at $T_{\rm N}$ is[43,44]

$$\delta C = \frac{5S(S+1)}{2S^2+2S+1} N_{\rm A} k_{\rm B}, \tag{3}$$

with $N_{\rm A}$ the Avogadro's constant and $k_{\rm B}$ the Boltzmann constant. Assuming $S = 1$ for our system, the derived δC should be $2N_{\rm A}k_{\rm B} \approx 16.6$ J/K·mol^{-1}. In the presence of Kondo coupling, the magnetic moment is partially screened, leading to a suppressed δC, which is directly related to $T_{\rm K}/T_{\rm N}$,[40,45] as depicted in Fig. 2(d). Therefore, according to the experimental value of δC derived from $C_{\rm mag}$, that is, about 13.3 J/K·mol^{-1} at $T_{\rm N}$, the Kondo temperature $T_{\rm K}$ can be estimated as ~ 8.1 K.

Given the key effect of intercalated V atoms in introducing the Kondo effect, it would be informative to compare the intercalate $V_{1/4}VS_2$ and the host compound VS_2. However, it is challenging to grow VS_2 because of self intercalation and contradicting properties have been observed so far.[46] Consequently, we have measured the specific heat of VSe_2 instead, an isoelectronic and isostructural compound of VS_2, shown in Appendix A. The Sommerfeld coefficient is found to be 46 mJ·K^{-2} per mol of V_4Se_8, smaller than that of V_5S_8. This difference offers additional evidence for enhanced electronic correlation by the Kondo coupling.

To get an idea of the strength of the electron correlation, we estimate the effective quasiparticle mass enhanced by the correlation by comparing the experimental Sommerfeld coefficient to that calculated from the Kohn–Sham model to density functional theory (DFT).[47] Within such a non-interacting electron model, the Sommerfeld coefficient can be estimated as $\gamma = \frac{1}{3}\pi^2 k_{\mathrm{B}}^2 N(\varepsilon_{\mathrm{F}})$, where k_{B} is the Boltzmann constant and $N(\varepsilon_{\mathrm{F}})$ is the density of states (DOS) per f.u. at the Fermi level ε_{F}. Our DFT calculation for the antiferromagetic phase of $\mathrm{V_5S_8}$ yields an electronic DOS of 6.6 states/eV/f.u., which translates to a Sommerfeld coefficient of only 16.8 $\mathrm{mJ{\cdot}K^{-2}{\cdot}mol^{-1}}$. To understand the difference between the experimental value and the calculated one here, it is necessary to first take into account the electron–phonon coupling which can enhance the Sommerfeld coefficient by a factor of $(1+\lambda_{\mathrm{ep}})$, where λ_{ep} is the mass enhancement factor due to the electron–phonon coupling.[48] A reasonable estimate of λ_{ep} is 1.19,[49] which was obtained in V metal. This leads to an enhanced Sommerfeld coefficient of 36.8 $\mathrm{mJ{\cdot}K^{-2}{\cdot}mol^{-1}}$. Thus, one can see that, even after accounting for the electron–phonon coupling effect, the theoretical value estimated from a quasiparticle picture is still markedly smaller than the experimental one. We attribute the remaining discrepancy to the mass enhancement effect due to electron correlations. That is, electron correlations give rise to an enhanced effective mass of 1.58 m_{e} with m_{e} being the bare electron mass. The details of our DFT calculation for the electronic DOS can be found in Appendix B.

2.5. Electrical resistivity

The temperature dependent resistivity of many metallic Kondo lattice materials exhibits characteristic features, such as a maximum, stemming from the Kondo scattering.[6,50] Figure 3 shows the resistivity for three $\mathrm{V_5S_8}$ single crystal samples A1, A2, and A3 grown from the same batch as sample A0. At 32 K, the resistivity exhibits a kink, which results from the antiferromagnetic transition. Above this temperature, there is an apparent hump at about 140 K, in stark contrast to a linear dependence commonly seen in metals.

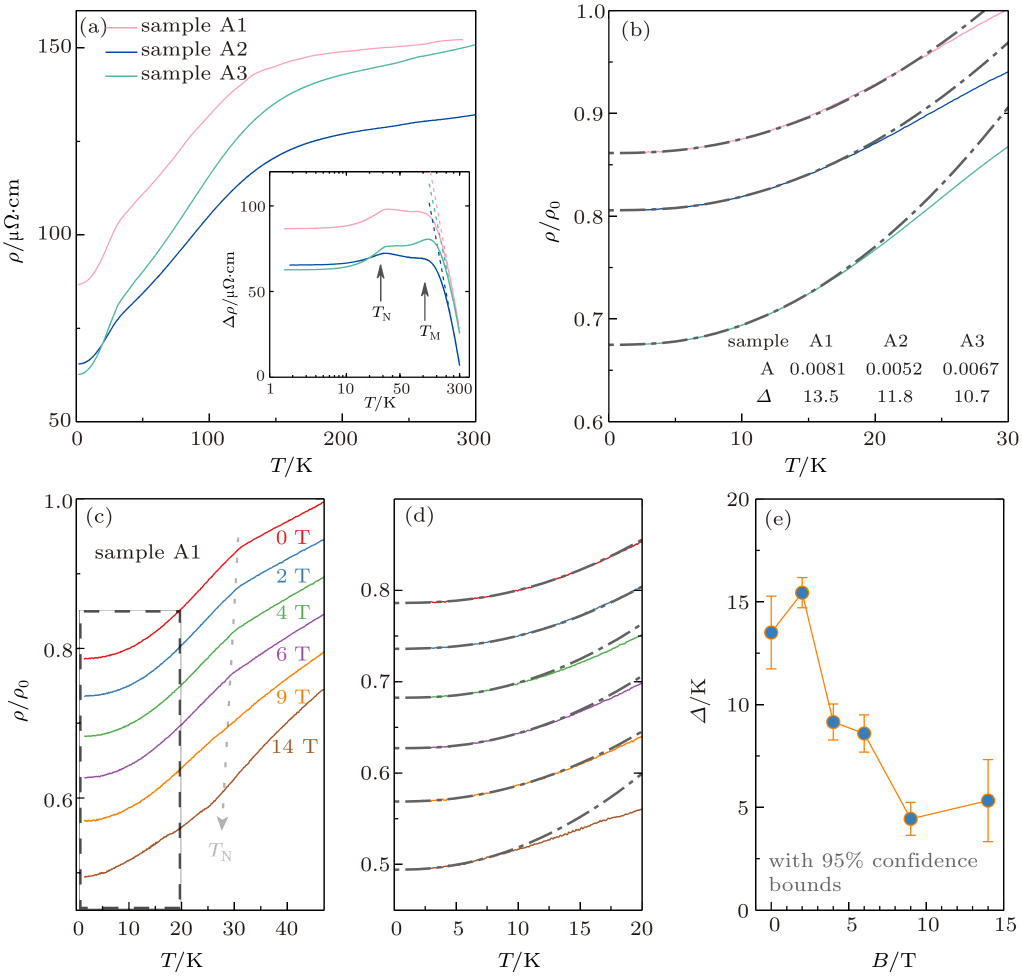

Fig. 3. Temperature dependence of resistivity. (a) The temperature-dependent resistivity of three samples. The inset illustrates the high-T resistivity after subtracting the non-magnetic ρ of $\mathrm{VSe_2}$ from that of $\mathrm{V_5S_8}$. The dotted lines are the $-\ln T$ fits. (b) Fits of the low-T ($T < 10$ K) resistivity $\rho/\rho(T = 50\ \mathrm{K})$ for the three samples in (a). The dashed lines indicate the fits using Eq. (4), the fitting results are shown in the lower right. The A and $\varDelta$ are in units of $\mathrm{\mu\Omega{\cdot}cm{\cdot}K^{-2}}$ and K, respectively. (c) Temperature dependent resistivity at different fields. (d), (e) The low-T resistivity $\rho/\rho(T = 50\ \mathrm{K})$ for sample A1 at different magnetic fields ($B \perp ab$ plane). Dot-dashed lines are fits to Eq. (4). (e) The fitted gap of sample A1 as a function of field. The curves in (b)–(d) are vertically shifted for clarity.

In fact, VSe_2 displays a typical metallic resistivity linear in T. We tentatively subtract the resistivity of VSe_2 from that of V_5S_8 to highlight the effect of intercalated atoms. As shown in the inset of Fig. 3(a), the broad maximum is evident. This feature has been observed in Kondo lattices and believed to originate from coherent Kondo scattering.[6,12,32,50] Although the crystal field may play a role, it often indicates collective local-moment deconfinement,[9,51,52] The deconfinement also manifests as a deviation from the Curie–Weiss behavior, which is observed at almost the same temperature in our experiments, see Fig. 1(d). On the high temperature side of the maximum, the resistivity roughly follows a $-\ln T$ dependence, consistent with the effect of incoherent Kondo scattering.

We now turn to the low temperature resistivity in the AFM state. In the magnetically ordered state, the strong decrease of the resistivity below T_N is caused by the reduction of spin-disorder scattering. In this case, the resistivity consists of both the electronic contribution and the magnon scattering term, and takes the form

$$\rho(T)=\rho_0+AT^2+b\frac{T}{\Delta}\left(1+2\left(\frac{T}{\Delta}\right)\right)\mathrm{e}^{-\Delta/T}, \tag{4}$$

where ρ_0 is the residual resistivity, the AT^2 term represents the Fermi liquid contribution, the last term is associated with the spin wave, and Δ is the spin wave gap.[12,53–55] The resistivity below 8 K can be well described by Eq. (4) (see Fig. 3(b)). The fitting parameters A and Δ are ~ 0.008 μΩ·cm·K^{-2} and ~ 13.5 K, respectively. The fitted gaps of all three samples A1, A2, A3 are in accordance with the gap fitted from the specific heat of A0. Moreover, A is found to be nearly independent of the magnetic field, which is consistent with the Fermi liquid contribution.[56,57] On the other hand, with increasing B, Δ decreases gradually from 15 K to 5 K (see Fig. 3(d)), which is similar to those observed in other antiferromagnetic Kondo systems.[54,58]

In strongly correlated systems, it has been found that the Kadowaki–Woods ratio, $r_{KW}=A/\gamma^2$, is significantly enhanced, around $a_0=1.0\times10^{-5}$ μΩ·cm(mol·K/mJ)^2.[59] Using the obtained Sommerfeld coefficient $\gamma=64$ mJ·K^{-2}·mol^{-1} and $A\sim0.008$ μΩ·cm·K^{-2}, we obtain $r_{KW}=0.20a_0$. This value is comparable to those in d-electron strongly correlated systems such as LiV_2O_4, V_2O_3, Sr_2RuO_4, $Na_{0.7}CoO_2$, etc.[33,60–63] and much larger than $0.04a_0$ in transition metals.[64]

The magnetoresistance shows features in agreement with the Kondo lattice. Figure 4(a) shows the magnetoresistance $MR=\frac{\rho(B)-\rho(0)}{\rho(0)}\times100\%$ at different temperatures. Below T_N, MR displays a sudden drop at the spin-flop transition, while in the high temperature paramagnetic state, MR follows a B^2 dependence, consistent with the spin fluctuation scattering.[29] Moreover, MR data in the paramagnetic state collapse onto a single curve when the field is scaled by $T+T^*$, where T^* is a characteristic temperature, as shown in Fig. 4(b). It is known that in a Kondo impurity model, the magnetoresistance follows the Schlottmann's relation $\frac{\rho(B)}{\rho(0)}=f[B/(T+T^*)]$.[65] The scaling behavior confirms the Kondo effect and has been observed in many Kondo lattices.[12,50,66] However, the best scaling of our data yields a negative $T^*=-6$ K. This sign is consistent with the positive CW temperature. Both the positive CW temperature and the negative T^* indicate the presence of ferromagnetic correlations.[12,50,66] A negative T^* has been reported in other antiferromagnetic heavy fermion compounds, such as $CeNiGe_3$,[50] $CeBi_2$,[66] and YbPtSn.[67]

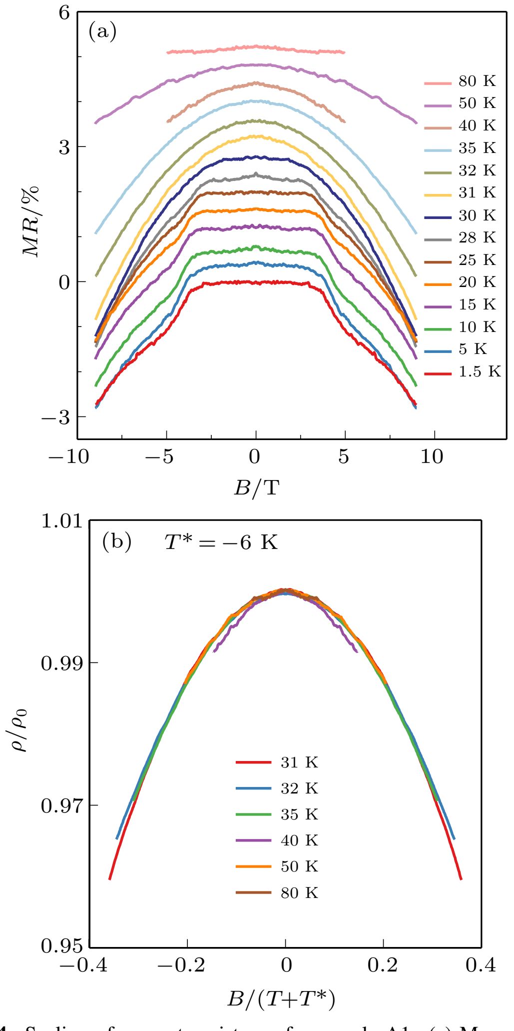

Fig. 4. Scaling of magnetoresistance for sample A1. (a) Magnetoresistance MR at various temperatures. The curves are vertically shifted for clarity. (b) Normalized resistivity versus $B/(T+T^*)$, where T^* is a scaling parameter.

2.6. Thermoelectric power

The thermoelectric properties of heavy fermion compounds share some common features.[68] Figure 5 shows the temperature-dependent thermopower S for V_5S_8 bulk single crystal. Instead of a linear T dependence as expected for ordinary metals, S shows a sign change at about 140 K, as well as a negative S minimum around 60 K. A change of sign is generally associated with a change of carrier type. However, this explanation is inconsistent with hole conduction inferred from Hall measurement in the whole temperature range (see Appendix A for details). In a Kondo lattice system, the interplay between the Kondo and crystal field effects gives rise to a broad peak in thermopower S at high temperatures. More prominently, with decreasing temperature, S changes its sign at $T = \alpha T_K$, where roughly $\alpha = 2.5$–10. After that, S displays an extremum and may change sign again in some compounds.[42,68–70] Our data agree with some of these essential features, e.g., a sign change and a negative peak. It is worth mentioning that the temperature of 140 K, at which S changes its sign, is very close to the temperature obtained from the resistivity maximum and deviation of the magnetic susceptibility from the CW law.

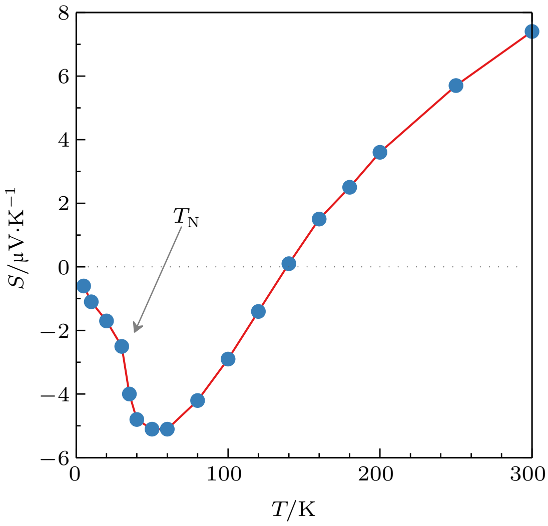

Fig. 5. Temperature-dependent thermopower S. S changes its sign at about 140 K and displays a negative minimum at 60 K.

3. Conclusion

Based on these observations, we conclude that itinerant electrons in V_5S_8 interact with intercalated local moments through the Kondo effect, giving rise to the enhancement of electron correlation. Under this picture, the magnetic susceptibility can be understood. The deviation from the CW law beginning at 140 K results from local-moment deconfinement by Kondo coupling, which has been seen in other heavy fermion compounds.[9,12,32,50–52,71,72] The reduction of the magnetic local moment at low temperatures is due to the Kondo screening, which, though strongly suppressed, persists in the AFM state.[6,10]

Our experiments strongly suggest that itinerant electrons in the intercalated material V_5S_8 are correlated. The results have demonstrated a means that can potentially bring a class of materials into the category of correlated electronic systems.

Appendix A: Additional experimental results

We studied the evolution of the Hall resistivity ρ_{xy} with temperature, as shown in Fig. A4(a). Here, ρ_{xy} includes two contributions, i.e., $\rho_{xy}(B) = R_0 B + R_{\mathrm{AHE}} \mu_0 M$, where R_0 and R_{AHE} are the ordinary and anomalous Hall coefficients, respectively, M is the magnetization, and μ_0 the vacuum permeability. So, the Hall coefficient can be expressed as $R_H = \rho_{xy}/B = R_0 + R_{\mathrm{AHE}} \mu_0 M/B$, namely, $R_H \propto \chi$. We plot R_H versus χ at different temperatures above T_N and find a good linear relation (see Fig. A4(b)). The intercept of the linear fit gives a positive value of $R_0 = 2.5 \times 10^{-4}\ \mathrm{cm}^3 \cdot \mathrm{C}^{-1}$, indicating a temperature independent holes carrier concentration of $n = 2.5 \times 10^{22}\ \mathrm{cm}^{-3}$.

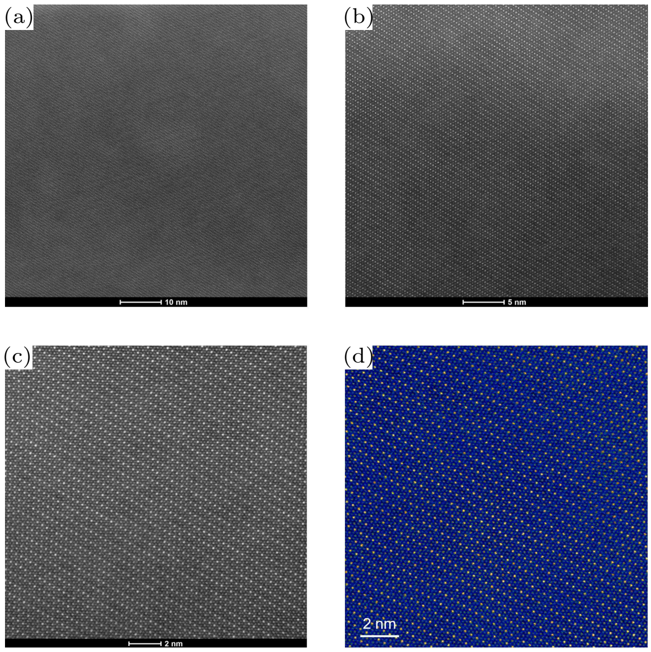

Fig. A1. HAADF-STEM images taken from different regions of a V_5S_8 single crystal. (a)–(c) HAADF-STEM images with different sizes. (d) Color-coded STEM image reveals clearly the V^I rectangular configuration (the brightest yellow dots).

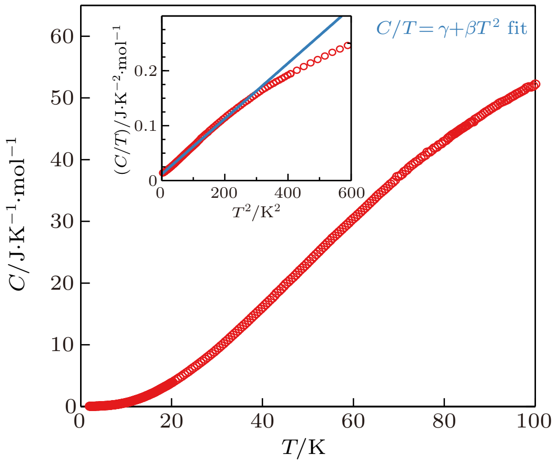

Fig. A2. Specific heat C of a 3.5 mg VSe_2 single crystal. VSe_2 displays no magnetic transition. At low temperatures, C/T is linearly dependent of T^2. A linear fit yields a Sommerfeld coefficient $\gamma \sim 11.5\ \mathrm{mJ \cdot K^{-2}}$ per mole of VSe_2 formula, shown in the inset.

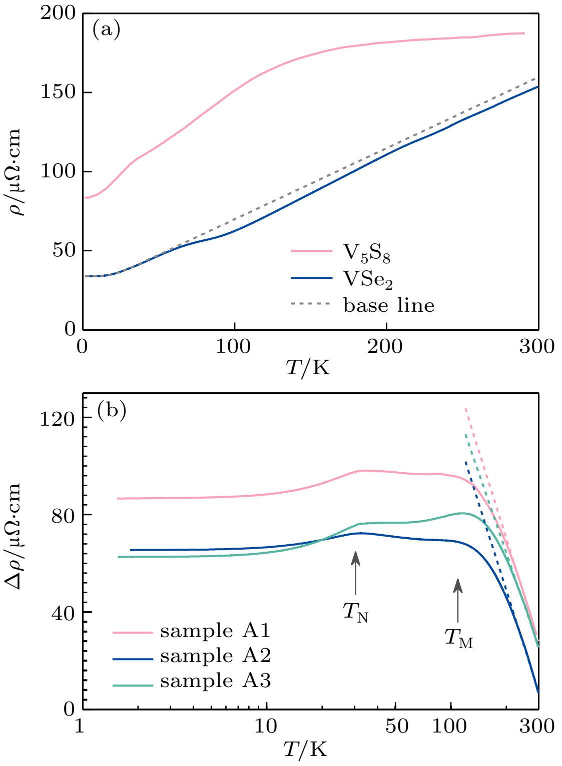

Fig. A3. (a) Comparison of the temperature dependent resistivity $\rho(T)$ between V_5S_8 and VSe_2. ρ versus T. VSe_2 displays a linear-T dependence, except for an anomaly at $\sim$ 90 K, which is due to a charge density wave transition. The dotted line is the baseline subtracted from the resistivity of V_5S_8 so as to highlight the contribution of the intercalation, $\Delta\rho$. (b) $\Delta\rho$ as a function of temperature.

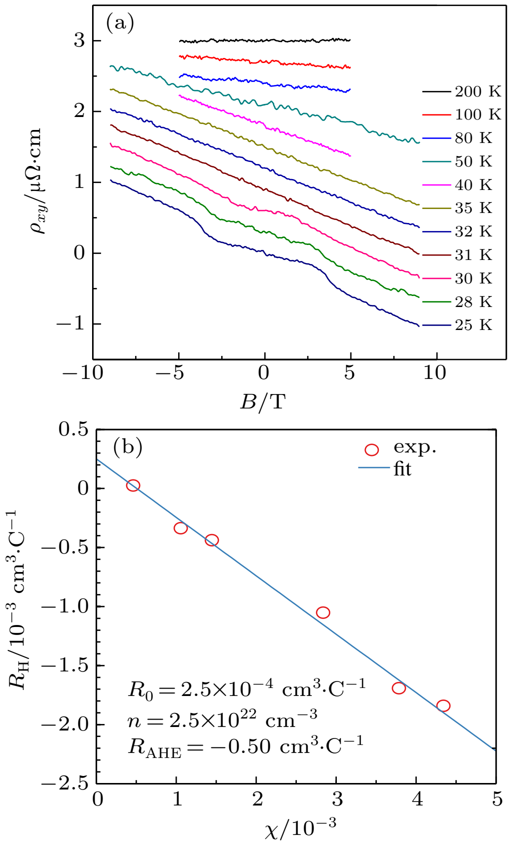

Fig. A4. Anomalous Hall effect and the carrier density of V_5S_8. (a) Hall resistivity ρ_{xy} (vertically shifted for clarity) at different temperatures. (b) Linear relation between the Hall coefficient R_H and the magnetic susceptibility χ above T_N. The blue line is a linear fit.

Appendix B: DFT calculations

We carried out density functional theory (DFT) calculations using the Perdew–Burke–Ernzerhof (PBE)[73] generalized gradient approximation as implemented in the all-electron first-principles code package Fritz Haber Institute *ab initio* molecular simulations (FHI-aims) package.[74] In accord with the experimental findings, the monoclinic crystal structure with antiferromagnetic ordering of the V^I atoms was used in our calculations. We employed an extended unit cell containing 8 formula unit cells (104 atoms in total), and a $6\times3\times3$ $\boldsymbol{k}$ grid (with the $\varGamma$ point included) for the Brillouin zone sampling. The FHI-aims "light" setting for the numerical grid integration and numerical atomic basis sets (5s4p2d1f for V and 4s3p1d for S) were used in the calculations. The unit cell geometry and atomic positions were fully relaxed, with resultant lattice parameters of $a = 22.62$ Å, $b = 6.62$ Å, $c = 11.37$ Å, and $\alpha = \gamma = 90°$, $\beta = 91.7°$. The calculated electronic density of states (DOS) is presented in Fig. B1, where one can see that the DOS at the Fermi level is dominated by contributions from V. The DOS value of 53.0 states/eV for the calculated supercell corresponds to $N(\varepsilon_F) = 6.6$ states/eV per formula unit cell. In Fig. B2 the projected DOSs of individual V species are presented, where the V^I atoms yield a pronounced peak just below the Fermi level, and contribute a major part of the spin polarization. A Mulliken charge analysis indicates that the local mangetic moments from V^I, V^{II}, and V^{III} atoms are $1.93\mu_B$, $0.15\mu_B$, and $0.04\mu_B$, respectively.

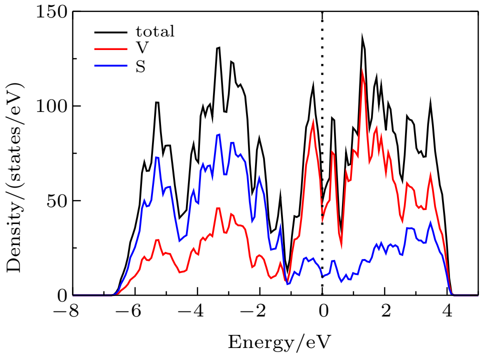

Fig. B1. Calculated total (black lines) and species-projected density of states (V: red lines; S: blue lines) of V_5S_8 bulk. The dash line at the 0 eV represents the Fermi level.

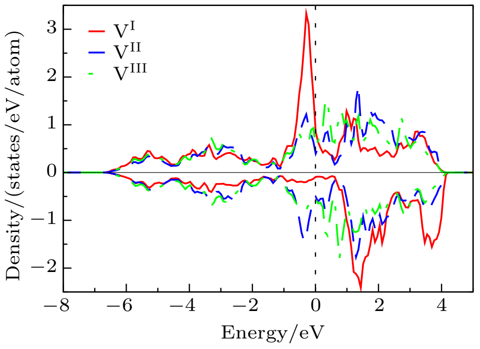

Fig. B2. The atom-projected density of states (PDOS) of V^I (solid red curve), V^{II} (dashed blue curve), and V^{III} (dot-dashed green curve) in V_5S_8 bulk.

References

[1] Lee P A, Nagaosa N and Wen X G 2006 *Rev. Mod. Phys.* **78** 17

[2] Stewart G R 1984 *Rev. Mod. Phys.* **56** 755

[3] Lee P A 2008 *Rep. Prog. Phys.* **71** 012501

[4] Doniach S 1977 *Physica B+C* **91** 231

[5] Ott H R, Rudigier H, Delsing P and Fisk Z 1984 *Phys. Rev. Lett.* **52** 1551

[6] Fisk Z, Ott H R, Rice T M and Smith J L 1986 *Nature* **320** 124

[7] Schröder A, Aeppli G, Coldea R, Adams M, Stockert O, Löhneysen H, Bucher E, Ramazashvili R and Coleman P 2000 *Nature* **407** 351

[8] Park T, Ronning F, Yuan H Q, Salamon M B, Movshovich R, Sarrao J L and Thompson J D 2006 *Nature* **440** 65

[9] Yang Y F, Fisk Z, Lee H O, Thompson J D and Pines D 2008 *Nature* **454** 611

[10] Si Q and Steglich F 2010 *Science* **329** 1161

[11] Kondo S, Johnston D C, Swenson C A, Borsa F, Mahajan A V, Miller L L, Gu T, Goldman A I, Maple M B, Gajewski D A, Freeman E J, Dilley N R, Dickey R P, Merrin J, Kojima K, Luke G M, Uemura Y J, Chmaissem O and Jorgensen J D 1997 *Phys. Rev. Lett.* **78** 3729

[12] Hossain Z, Hamashima S, Umeo K, Takabatake T, Geibel C and Steglich F 2000 *Phys. Rev. B* **62** 8950

[13] Cheng J G, Zhou J S, Yang Y F, Zhou H D, Matsubayashi K, Uwatoko Y, MacDonald A and Goodenough J B 2013 *Phys. Rev. Lett.* **111** 176403

[14] Marseglia E A 1983 *Int. Rev. Phys. Chem.* **3** 177

[15] Friend R and Yoffe A 1987 *Adv. Phys.* **36** 1

[16] Dresselhaus M S and Dresselhaus G 2002 *Adv. Phys.* **51** 1

[17] Chhowalla M, Shin H S, Eda G, Li L J, Loh K P and Zhang H 2013 *Nat. Chem.* **5** 263

[18] Jung Y, Zhou Y and Cha J J 2016 *Inorg. Chem. Front.* **3** 452

[19] Silbernagel B G, Levy R B and Gamble F R 1975 *Phys. Rev. B* **11** 4563

[20] Fujimori A, Saeki M and Nozaki H 1991 *Phys. Rev. B* **44** 163

[21] Murphy D W, Cros C, Salvo F J D and Waszczak J V 1977 *Inorg. Chem.* **16** 3027

[22] Nozaki H, Umehara M, Ishizawa Y, Saeki M, Mizoguchi T and Nakahira M 1978 *J. Phys. Chem. Solids* **39** 851

[23] Vries A D and Haas C 1973 *J. Phys. Chem. Solids* **34** 651

[24] Nishihara H, Yasuoka H, Oka Y, Kosuge K and Kachi S 1977 *J. Phys. Soc. Jpn.* **42** 787

[25] Kitaoka Y and Yasuoka H 1980 *J. Phys. Soc. Jpn.* **48** 1949

[26] Katsuta H, McLellan R B and Suzuki K 1979 *J. Phys. Chem. Solids* **40** 1089

[27] Nakanishi M, Yoshimura K, Kosuge K, Goto T, Fujii T and Takada J 2000 *J. Magn. Magn. Mater.* **221** 301

[28] Funahashi S, Nozaki H and Kawada I 1981 *J. Phys. Chem. Solids* **42** 1009

[29] Niu J, Yan B, Ji Q, Liu Z, Li M, Gao P, Zhang Y, Yu D and Wu X 2017 *Phys. Rev. B* **96** 075402

[30] Barua S, Hatnean M C, Lees M R and Balakrishnan G 2017 *Sci. Rep.* **7** 10964

[31] Liu H, Xue Y, Shi J A, Guzman R A, Zhang P, Zhou Z, He Y, Bian C, Wu L, Ma R et al. 2019 *Nano Lett.* **19** 8572

[32] Hossain Z, Ohmoto H, Umeo K, Iga F, Suzuki T, Takabatake T, Takamoto N and Kindo K 1999 *Phys. Rev. B* **60** 10383

[33] Li S Y, Taillefer L, Hawthorn D G, Tanatar M A, Paglione J, Sutherland M, Hill R W, Wang C H and Chen X H 2004 *Phys. Rev. Lett.* **93** 056401

[34] Andersen N H and Smith H 1979 *Phys. Rev. B* **19** 384

[35] Lashley J C, Stevens R, Crawford M K, Boerio-Goates J, Woodfield B F, Qiu Y, Lynn J W, Goddard P A and Fisher R A 2008 *Phys. Rev. B* **78** 104406

[36] Falkowski M, Kowalczyk A and Toliński T 2011 *J. Alloys Compd.* **509** 6135

[37] Toliński T, Kowalczyk A, Szewczyk A and Gutowska M 2006 *J. Phys.: Condens. Matter* **18** 3435

[38] Svoboda P, Vejpravová J, Kim-Ngan N T and Kaysel F 2004 *J. Magnet. Magnet. Mater.* **272–276** 595

[39] Schotte K and Schotte U 1975 *Phys. Lett. A* **55** 38

[40] Bredl C D, Steglich F and Schotte K D 1978 *Zeitschrift Für Physik B Condensed Matter* **29** 327

[41] Kawabata J, Takabatake T, Umeo K and Muro Y 2014 *Phys. Rev. B* **89** 094404

[42] Hodovanets H, Bud'ko S L, Straszheim W E, Taufour V, Mun E D, Kim H, Flint R and Canfield P C 2015 *Phys. Rev. Lett.* **114** 236601

[43] Mattis D C 1985 *Theory of Magnetism II: Thermodynamics and statistical mechanics* (Berlin and New York: Springer-Verlag) p. 22

[44] Blanco J A, Gignoux D and Schmitt D 1991 *Phys. Rev. B* **43** 13145

[45] Blanco J A, de Podesta M, Espeso J I, Gomez Sal J C, Lester C, McEwen K A, Patrikios N and Rodriguez Fernandez J 1994 *Phys. Rev. B* **49** 15126

[46] Gauzzi A, Sellam A, Rousse G, Klein Y, Taverna D, Giura P, Calandra M, Loupias G, Gozzo F, Gilioli E, Bolzoni F, Allodi G, De Renzi R, Calestani G L and Roy P 2014 *Phys. Rev. B* **89** 235125

[47] Kohn W and Sham L J 1965 *Phys. Rev.* **140** A1133

[48] Beck P A and Claus H 1970 *J. Res. Nat. Bur. Stand.* **A 74** 449

[49] Savrasov S Y and Savrasov D Y 1996 *Phys. Rev. B* **54** 16487

[50] Pikul A P, Kaczorowski D, Plackowski T, Czopnik A, Michor H, Bauer E, Hilscher G, Rogl P and Grin Y 2003 *Phys. Rev. B* **67** 224417

[51] Yang Y F and David P 2012 *Proc. Natl. Acad. Sci. USA* **109** E3060

[52] Yang Y F 2016 *Rep. Prog. Phys.* **79** 074501

[53] Becker B, Ramakrishnan S, Menovsky A A, Nieuwenhuys G J and Mydosh J A 1997 *Phys. Rev. Lett.* **78** 1347

[54] Mentink S A M, Mason T E, Süllow S, Nieuwenhuys G J, Menovsky A A, Mydosh J A and Perenboom J A A J 1996 *Phys. Rev. B* **53** R6014

[55] Andersen N H 1980 *Crystalline electric field and structural effects in f-electron systems* (New York and London: Plenum) p. 375

[56] Raquet B, Viret M, Sondergard E, Cespedes O and Mamy R 2002 *Phys. Rev. B* **66** 024433

[57] Madduri P V P and Kaul S N 2017 *Phys. Rev. B* **95** 184402

[58] Jobiliong E, Brooks J S, Choi E S, Lee H and Fisk Z 2005 *Phys. Rev. B* **72** 104428

[59] Kadowaki K and Woods S 1986 *Solid State Commun.* **58** 507

[60] McWhan D B, Remeika J P, Bader S D, Triplett B B and Phillips N E 1973 *Phys. Rev. B* **7** 3079

[61] Maeno Y, Yoshida K, Hashimoto H, Nishizaki S, ichi Ikeda S, Nohara M, Fujita T, Mackenzie A, Hussey N, Bednorz J and Lichtenberg F 1997 *J. Phys. Soc. Jpn.* **66** 1405

[62] Urano C, Nohara M, Kondo S, Sakai F, Takagi H, Shiraki T and Okubo T 2000 *Phys. Rev. Lett.* **85** 1052

[63] Miyake K, Matsuura T and Varma C 1989 *Solid State Commun.* **71** 1149

[64] Jacko A C, Fjærestad J O and Powell B J 1989 *Nat. Phys.* **5** 422

[65] Schlottmann P 1989 *Phys. Rep.* **181** 1

[66] Zhou W, Xu C Q, Li B, Sankar R, Zhang F M, Qian B, Cao C, Dai J H, Lu J, Jiang W X, Qian D and Xu X 2018 *Phys. Rev. B* **97** 195120

[67] Pietri R, Andraka B, Kaczorowski D, Leithe-Jasper A, and Rogl P 2000 *Phys. Rev. B* **61** 12169

[68] Zlatić V, Horvatić B, Milat I, Coqblin B, Czycholl G and Grenzebach C 2003 *Phys. Rev. B* **68** 104432

[69] Jaccard D, Behnia K and Sierro J 1992 *Phys. Lett. A* **163** 475

[70] Ren Z, Scheerer G W, Lapertot G and Jaccard D 2016 *Phys. Rev. B* **94** 024522

[71] Fan Y T, Lee W H and Chen Y Y 2004 *Phys. Rev. B* **69** 132401

[72] Szlawska M and Kaczorowski D 2012 *Phys. Rev. B* **85** 134423

[73] Perdew J P, Burke K and Ernzerhof M 1996 *Phys. Rev. Lett.* **77** 3865

[74] Blum V, Gehrke R, Hanke F, Havu P, Havu V, Ren X G, Reuter K and Scheffler M 2009 *Comput. Phys. Commun.* **180** 2175